AGU PUBLICATIONS

JGR

Journal of Geophysical Research: Planets

RESEARCH ARTICLE

10.1002/2015JE004821

Key Points:

- We examine inertial effects on tidal deformation of icy satellites with a solid lid
- A resonance occurs when a subsurface ocean is thin
- The resonant configuration strongly depends on the properties of the icy shell

Supporting Information:

- Text S1 and Captions of Data Sets S1–S9
- Data Set S1
- Data Set S2
- Data Set S3
- Data Set S4
- Data Set S5
- Data Set S6
- Data Set S7
- Data Set S8
- Data Set S9

Correspondence to:
S. Kamata,
kamata@mail.sci.hokudai.ac.jp

Citation:
Kamata, S., I. Matsuyama, and F. Nimmo (2015), Tidal resonance in icy satellites with subsurface oceans, *J. Geophys. Res. Planets*, *120*, 1528–1542, doi:10.1002/2015JE004821.

Received 17 MAR 2015
Accepted 18 AUG 2015
Accepted article online 24 AUG 2015
Published online 24 SEP 2015

Tidal resonance in icy satellites with subsurface oceans

Shunichi Kamata[1], Isamu Matsuyama[2], and Francis Nimmo[3]

[1]Creative Research Institution, Hokkaido University, Sapporo, Japan, [2]Department of Planetary Sciences, Lunar and Planetary Laboratory, University of Arizona, Tucson, Arizona, USA, [3]Department of Earth and Planetary Sciences, University of California, Santa Cruz, California, USA

Abstract Tidal dissipation is a major heat source for the icy satellites of the giant planets. Several icy satellites likely possess a subsurface ocean underneath an ice shell. Previous studies of tidal dissipation on icy satellites, however, have either assumed a static ocean or ignored the effect of the ice lid on subsurface ocean dynamics. In this study, we examine inertial effects on tidal deformation of satellites with a dynamic ocean overlain by an ice lid based on viscoelasto-gravitational theory. Although ocean dynamics is treated in a simplified fashion, we find a resonant configuration when the phase velocity of ocean gravity waves is similar to that of the tidal bulge. This condition is achieved when a subsurface ocean is thin (<1 km). The enhanced deformation (increased h_2 and k_2 Love numbers) near the resonant configuration would lead to enhanced tidal heating in the solid lid. A static ocean formulation gives an accurate result only if the ocean thickness is much larger than the resonant thickness. The resonant configuration strongly depends on the properties of the shell, demonstrating the importance of the presence of a shell on tidal dissipation.

1. Introduction

Tidal dissipation is one of the major heat sources for the evolution of planetary bodies, particularly the satellites of the giant planets [e.g., *Schubert et al.*, 1986, 2010]. Most of the satellites of Jupiter and Saturn are covered by an icy shell because of the low surface temperature. Based on internal thermal and structural modeling, large icy satellites, such as Europa and Titan, are expected to possess an internal ocean underneath an icy shell [e.g., *Hussmann et al.*, 2007]. This expectation is supported from observational data by the Galileo and Cassini spacecraft and by the Hubble Space Telescope [e.g., *Kivelson et al.*, 2000, 2002; *Iess et al.*, 2012; *Saur et al.*, 2015]. Observations by the Cassini spacecraft further suggest that even small satellites of Saturn, such as Enceladus and perhaps Mimas, have a subsurface ocean [e.g., *Iess et al.*, 2014; *Tajeddine et al.*, 2014]. Moreover, model calculations suggest that Pluto may also possess a subsurface ocean [e.g., *Schubert et al.*, 2010; *Robuchon and Nimmo*, 2011], and tidal dissipation due to the orbital motion of its largest satellite, Charon, may have heated Pluto in the past [*Barr and Collins*, 2015]. Thus, a detailed investigation of the evolution of planetary bodies in the outer solar system should consider tidal dissipation using an interior model consisting of an outer solid layer, internal liquid layer(s), and a solid (or liquid) core.

Previous studies of tidal dissipation in icy satellites using spherically symmetric models can be classified into two types: those considering tidal dissipation in the solid part and those considering tidal dissipation in the ocean. The former studies consider deformation of a solid planetary body due to periodic tidal force [e.g., *Moore and Schubert*, 2000; *Tobie et al.*, 2005; *Roberts and Nimmo*, 2008; *Beuthe*, 2015a]. In such studies, the equation system based on elasto-gravitational theory (widely used to investigate free oscillation problems at seismic frequencies [e.g., *Love*, 1911; *Alterman et al.*, 1959; *Takeuchi and Saito*, 1972]) are used because this equation system can be easily applied to a viscoelastic body. An application of Fourier transformation to the equations for tidal deformation on a viscoelastic body leads to the same form of the equations for deformation on an elastic body (i.e., the correspondence principle) [e.g., *Zschau*, 1978]. Although this formulation has been applied to many satellites and planets, the effect of an internal liquid layer on tidal deformation has usually been treated in a simplified fashion, as we discuss below.

The other type of studies, on the other hand, investigate tidal dissipation considering ocean dynamics using the Laplace tidal equations [e.g., *Tyler*, 2008; *Chen et al.*, 2014]. Such studies reveal that a thin ocean (i.e., <1 km for most cases) in icy satellites leads to a resonance, resulting in potentially large heat production [e.g., *Tyler*, 2011; *Matsuyama*, 2014]. This finding is important not only because the ocean thickness in icy satellites is poorly constrained but also because the ocean thickness may vary largely with time. One important assumption in these models is that the surface topography follows an equipotential surface. This requires either that the ocean is at the surface or that the ice shell overlying the ocean is soft. In reality, none of the icy satellites has a surface ocean, and in some cases (such as Titan [e.g., *Hemingway et al.*, 2013]) the ice shell may not be sufficiently soft because the viscosity of ice is very high at low temperatures [e.g., *Schulson and Duval*, 2009]. Prior to the work presented here, the influence of an overlying solid lid (i.e., the top icy shell) on ocean tidal dissipation has not been investigated.

In this study, we revisit the viscoelasto-gravitational theory and obtain a comprehensive equation system that can account for a thin subsurface ocean in viscoelastic planets (and satellites) (section 2). We then apply our theory to icy satellites and investigate the effect of an icy shell on the resonant configuration (sections 3 and 4). Because we are most interested in identifying what factors control the resonant response, our satellite models are deliberately simplified. However, the use of more realistic structural models will not affect our conclusions in a qualitative sense.

2. Theory

We follow the well-established elasto-gravitational theory considering deformation of a spherically symmetric, nonrotating, elastic, and isotropic body [e.g., *Love*, 1911]. In this theory, three equations are solved: the equation of momentum conservation, the Poisson equation for the gravitational field, and the constitutive equation. This theory can be applied not only for an elastic body but also for a viscoelastic body by adopting an appropriate constitutive equation. First, the equation of momentum conservation ignoring centrifugal and Coriolis forces is given by

$$\rho \frac{\mathrm{d}^2 \boldsymbol{u}}{\mathrm{d}t^2} = \boldsymbol{\nabla} \cdot \sigma + \rho \boldsymbol{F}, \tag{1}$$

where $\boldsymbol{u}$ is the displacement vector, σ is stress tensor, $\boldsymbol{F}$ is the sum of all the forces per unit mass acting on the body, t is time, and ρ is density, respectively. Second, the Poisson equation for the gravitational field is given by

$$\boldsymbol{\nabla}^2 \Phi = -4\pi G \boldsymbol{\nabla} \cdot (\rho \boldsymbol{u}), \tag{2}$$

where Φ is gravitational potential and G is the gravitational constant, respectively. Third, the constitutive equation for a Maxwell body is given by

$$\frac{\mathrm{d}\sigma_{ij}}{\mathrm{d}t} + \frac{\eta}{\mu}\left(\sigma_{ij} - \frac{\sigma_{kk}}{3}\delta_{ij}\right) = \lambda \frac{\mathrm{d}e_{kk}}{\mathrm{d}t}\delta_{ij} + 2\mu \frac{\mathrm{d}e_{ij}}{\mathrm{d}t}, \tag{3}$$

where e is strain tensor, δ_{ij} is the unit diagonal tensor, η is viscosity, μ is shear modulus, and λ is the first Lamé's parameter, respectively.

To calculate periodic deformation, a Fourier transform is applied to the three equations above assuming that the unknown variables ($\boldsymbol{u}$, σ, and Φ) oscillate with a frequency of ω; $\mathrm{d}/\mathrm{d}t$ is replaced with $i\omega$ where i is the imaginary number. Then, a spherical harmonic expansion is applied to such Fourier transformed equations, leading to a six-component differential equation system. In this study, we follow the formulation by *Takeuchi and Saito* [1972]. The equation system for a compressible solid layer is given by

$$\frac{\mathrm{d}y_1}{\mathrm{d}r} = -\frac{2\tilde{\lambda}}{(\tilde{\lambda}+2\tilde{\mu})r}y_1 + \frac{1}{\tilde{\lambda}+2\tilde{\mu}}y_2 + \frac{n(n+1)\tilde{\lambda}}{(\tilde{\lambda}+2\tilde{\mu})r}y_3, \tag{4}$$

$$\begin{aligned}\frac{\mathrm{d}y_2}{\mathrm{d}r} = &\left\{-\omega^2\rho + \frac{12\kappa\tilde{\mu}}{(\tilde{\lambda}+2\tilde{\mu})r^2} - \frac{4\rho g}{r}\right\}y_1 - \frac{4\tilde{\mu}}{(\tilde{\lambda}+2\tilde{\mu})r}y_2 \\ &+ \frac{n(n+1)}{r}\left\{\rho g - \frac{6\kappa\tilde{\mu}}{(\tilde{\lambda}+2\tilde{\mu})r}\right\}y_3 + \frac{n(n+1)}{r}y_4 + \frac{(n+1)\rho}{r}y_5 - \rho y_6,\end{aligned} \tag{5}$$

$$\frac{\mathrm{d}y_3}{\mathrm{d}r} = -\frac{1}{r}y_1 + \frac{1}{r}y_3 + \frac{1}{\tilde{\mu}}y_4, \tag{6}$$

$$\frac{dy_4}{dr} = \left\{ \frac{\rho g}{r} - \frac{6\kappa\tilde{\mu}}{(\tilde{\lambda}+2\tilde{\mu})r^2} \right\} y_1 - \frac{\tilde{\lambda}}{(\tilde{\lambda}+2\tilde{\mu})r} y_2 + \left\{ -\omega^2\rho + \frac{4n(n+1)(\tilde{\lambda}+\tilde{\mu})\tilde{\mu}}{(\tilde{\lambda}+2\tilde{\mu})r^2} - \frac{2\tilde{\mu}}{r^2} \right\} y_3 - \frac{3}{r}y_4 - \frac{\rho}{r}y_5, \tag{7}$$

$$\frac{dy_5}{dr} = 4\pi G\rho y_1 - \frac{n+1}{r}y_5 + y_6, \text{ and} \tag{8}$$

$$\frac{dy_6}{dr} = \frac{4\pi(n+1)G\rho}{r}y_1 - \frac{4\pi n(n+1)G\rho}{r}y_3 + \frac{n-1}{r}y_6, \tag{9}$$

where n is spherical harmonic degree, r is radial distance from the center, and $\kappa = \lambda + 2\mu/3$ is bulk modulus, respectively. The unknown variable y_1 is the coefficient for the vertical displacement, y_2 is the vertical stress, y_3 is the tangential displacement, y_4 is the tangential stress, y_5 is the gravitational potential perturbation, and y_6 is the "potential stress" [*Sabadini and Vermeersen*, 2004], respectively. Note that y is a complex variable. The complex elastic moduli are given by

$$\tilde{\lambda} = \frac{i\omega\lambda + \mu\kappa/\eta}{i\omega + \mu/\eta}, \quad \tilde{\mu} = \frac{i\omega\mu}{i\omega + \mu/\eta}. \tag{10}$$

See Appendix A for the expression under the incompressible limit (i.e., $\lambda \to \infty$). We note that there are differences in definitions of y between *Takeuchi and Saito* [1972] and some other studies [e.g., *Sabadini and Vermeersen*, 2004; *Roberts and Nimmo*, 2008]; y_2 and y_3 are interchanged, and the sign of y_5 and y_6 is opposite. We also found a typo in the equation for dy_6/dr in *Roberts and Nimmo* [2008].

The differential equation system above assumes $\mu \neq 0$. The equation system for a compressible liquid layer ($\mu = 0$) is a four-component system given by

$$\frac{dy_1}{dr} = \left\{ -\frac{2}{r} + \frac{n(n+1)g}{\omega^2 r^2} \right\} y_1 + \left\{ \frac{1}{\lambda} - \frac{n(n+1)}{\omega^2\rho r^2} \right\} y_2 - \frac{n(n+1)}{\omega^2 r^2} y_5, \tag{11}$$

$$\frac{dy_2}{dr} = \left\{ -\omega^2\rho - \frac{4\rho g}{r} + \frac{n(n+1)\rho g^2}{\omega^2 r^2} \right\} y_1 - \frac{n(n+1)g}{\omega^2 r^2} y_2 + \frac{(n+1)\rho}{r}\left(1 - \frac{ng}{\omega^2 r}\right) y_5 - \rho y_6, \tag{12}$$

$$\frac{dy_5}{dr} = 4\pi G\rho y_1 - \frac{n+1}{r}y_5 + y_6, \text{ and} \tag{13}$$

$$\frac{dy_6}{dr} = \frac{4\pi(n+1)G\rho}{r}\left(1 - \frac{ng}{\omega^2 r}\right) y_1 + \frac{4\pi n(n+1)G}{\omega^2 r^2} y_2 + \frac{4\pi n(n+1)\rho G}{\omega^2 r^2} y_5 + \frac{n-1}{r} y_6. \tag{14}$$

Note that $\tilde{\lambda} = \lambda$ when $\mu = 0$ (see equation (10)). Inside a liquid layer, the tangential stress y_4 is always zero, but tangential displacement y_3 can be determined from the equation below;

$$y_3 = \frac{1}{\omega^2\rho r}\left(\rho g y_1 - y_2 - \rho y_5\right). \tag{15}$$

The differential equations above are integrated numerically upward assuming a small homogeneous core (see Appendix B). The boundary conditions between solid-liquid interfaces can be found in *Takeuchi and Saito* [1972].

The coefficients for the solutions are determined from the boundary condition at the surface, which is given by

$$y_2 = 0, \quad y_4 = 0, \quad y_6 = \frac{2n+1}{r_s}\Phi_t, \tag{16}$$

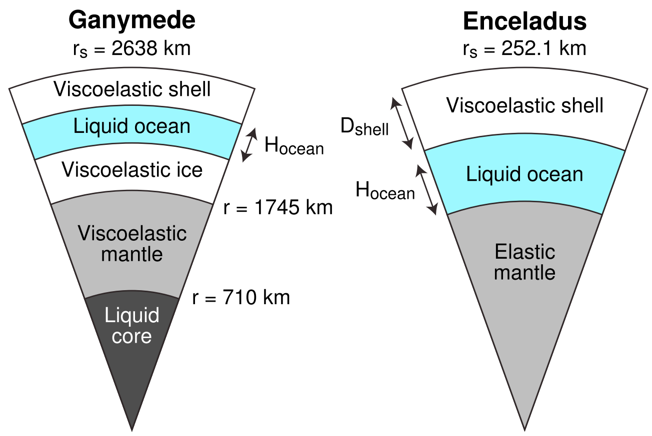

Figure 1. Interior structure models adopted. An incompressible five-layer and three-layer model is used for Ganymede and Enceladus, respectively.

where r_s is the radius of a body and Φ_t is tidal potential at the surface. We note that this formulation can also be applied to a model with a surface ocean. In this case, the surface boundary condition is given by

$$y_2 = 0, \quad y_6 = \frac{2n+1}{r_s}\Phi_t. \tag{17}$$

The equation system for a liquid layer (i.e., equations (11)–(14)) is significantly different from those used in several previous studies based on (visco) elasto-gravitational theory [e.g., *Saito*, 1974; *Jara-Orué and Vermeersen*, 2011; *Harada et al.*, 2014]. Specifically, these studies use a two-component equation system for a liquid layer. This two-component equation system can be obtained under a quasi-static assumption; $\omega^2 = 0$, which is equivalent to setting the left-hand side of equation (1) to zero [*Saito*, 1974]. Although this formulation has been used by many tidal dissipation studies, it may lead to a large error when the ocean is thin even if the frequency is low (see section 3). In the following, we call the formulation using this two-component equation system a static formulation while a four-component system is referred to as a dynamic formulation. Note that ocean dynamics is not completely included in this "dynamic formulation"; Coriolis forces, for example, are not taken into account.

The dynamical formulation discussed above has smaller model requirements compared to other spectral schemes. For example, this formulation can handle a liquid (i.e., $\mu = 0$) layer; such a layer need not be approximated as a solid layer with a low (but nonzero) rigidity [*Roberts and Nimmo*, 2008]. This is important because if a "liquid" layer is treated as such, no resonance would be found. In addition, the core needs not to be liquid (see Appendix B). This formulation can also be applied to cases with a high tidal frequency and to situations with a density contrast between an ocean and a shell, which cannot be handled by a method based on a membrane theory [*Beuthe*, 2015a]. A more recent study calculates tidal Love numbers using a formulation similar to ours [*Beuthe*, 2015b], though the inertial term for solid layers and compressibility in liquid layers are neglected. We note that the formulation discussed above is based on a classical spectral theory assuming a spherically symmetric body and small-amplitude deformations. Consequently, to incorporate lateral variations of interior properties, a fully numerical approach is necessary [e.g., *Tobie et al.*, 2008; *A et al.*, 2013].

3. Tidal Resonance

In this section, we show that a dynamic formulation leads to a resonance under a specific condition while a static formulation does not lead to any resonances. Here we use a five-layer Ganymede model by *Moore and Schubert* [2003]. Ganymede is assumed to consist of a viscoelastic icy shell, a liquid subsurface ocean, a viscoelastic high-pressure icy layer, a viscoelastic rocky mantle, and a liquid metallic core (Figure 1, left). All solid layers are assumed to be (Maxwellian) viscoelastic. Table 1 lists the parameters adopted. The ocean thickness H_{ocean} and the ice viscosity η_{ice} are free parameters. The central depth of the ocean is fixed at a depth of 145 km; the top shell thickness is thus given by $145 - H_{ocean}/2$ km. We note that this model gives a surface gravitational acceleration $\sim$1.24 m s^{-2}, which is $\sim$13% smaller than the actual value [*Anderson et al.*, 1996]. Also, the radius is slightly larger than the actual value [e.g., *Schubert et al.*, 2004]. Nevertheless, we use these values adopted in a previous study because a direct comparison with previously reported results can be used to validate our code.

Figure 2 shows the absolute value of the degree 2 Love number, h_2, as a function of ice viscosity, η_{ice}. Here h_2 is calculated from $h_2 = y_1(r_s)g(r_s)/\Phi_t$. Results obtained using a dynamic formulation and a static formulation are shown in Figures 2a and 2b, respectively. Values of h_2 for $H_{ocean} = 0$ (i.e., no ocean), 20, and 200 km reported by *Moore and Schubert* [2003] are in agreement with those obtained from our code both for Figures 2a and 2b. This result not only demonstrates the validity of our code but also indicates that a static formulation leads to accurate results when there is no ocean or when the ocean is thick (i.e., $\geq$20 km). On the other hand,

Table 1. Model Parameters for Ganymede

Symbol	Quantity	Value	Unit
r_s	Radius of Ganymede	2638	km
r_m	Radius of the mantle	1745	km
r_c	Radius of the core	710	km
ρ_{H_2O}	Density of ice and ocean	1050	kg m^{-3}
ρ_m	Density of the mantle	3100	kg m^{-3}
ρ_c	Density of the core	5150	kg m^{-3}
μ_s	Rigidity of the shell	10	GPa
μ_m	Rigidity of the mantle	100	GPa
μ_c	Rigidity of the core	0	GPa
η_m	Viscosity of the mantle	10^{20}	Pa s
η_c	Viscosity of the core	0	Pa s
$\omega_{\rm orb}$	Orbital frequency	1.016×10^{-5}	rad s^{-1}

when the ocean is thin (i.e., $0 < H_{\rm ocean} \le 1$ km), a large difference in h_2 between Figure 2a and Figure 2b can be seen, indicating that a static formulation can lead to large errors even when the frequency is low.

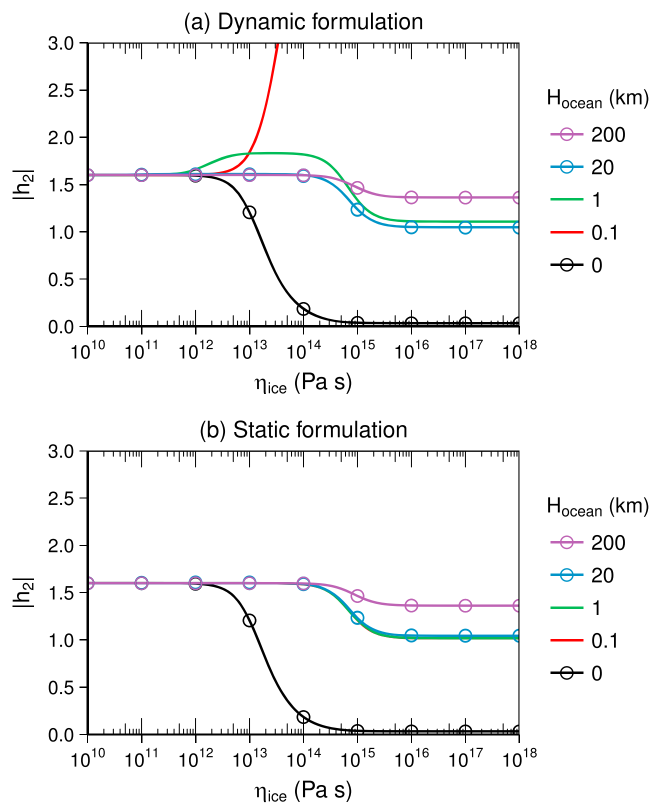

Figure 2. Absolute value of the degree 2 Love number h_2 as a function of ice viscosity for a Ganymede model. Results obtained using (a) a dynamic formulation and (b) a static formulation, respectively, are shown. Previously reported results for ocean thicknesses ($H_{\rm ocean}$) 0, 20, and 200 km by *Moore and Schubert* [2003] are illustrated with circles, showing a good agreement with our results. While results for Figures 2a and 2b under $H_{\rm ocean} > 1$ km or $H_{\rm ocean} = 0$ km are the same, a clear difference between results can be seen when $0 < H_{\rm ocean} \le 1$ km. Note that $|h_2| > 3$ for $H_{\rm ocean} = 0.1$ km and $\eta_{\rm ice} > 4 \times 10^{13}$ Pa s when a dynamical formulation is used.

Figure 3 shows the real part of h_2 as a function of ocean thickness, $H_{\rm ocean}$. This figure clearly shows that a dynamic formulation leads to a resonance when $H_{\rm ocean} \sim 0.1$ km. We found that this thickness is close to the thickness that results in a phase velocity of gravity waves $v_{\rm grav}$ similar to the phase velocity of degree 2 tidal deformation $v_{\rm tidal}$. The phase velocity for a shallow surface water wave is given by $v_{\rm grav} \approx \sqrt{gH_{\rm ocean}}$ when curvature is neglected. The phase velocity of degree 2 tidal deformation, on the other hand, is defined as $v_{\rm tidal} = \omega_{\rm orb}/k$, where $\omega_{\rm orb}$ is the orbital frequency and k is wave number, respectively. The wave number k for degree 2 deformation is given by $k = (n+1/2)/r$, where $n(=2)$ is spherical harmonic degree [*Dahlen and Tromp*, 1998]. Consequently, a resonant thickness $H_{\rm res}$ is given by

$$H_{\rm res} \approx \frac{r^2 \omega_{\rm orb}^2}{(n+1/2)^2 g} \approx 81.8 \text{ m}. \quad (18)$$

Here we use the central radius of the ocean (i.e., a depth of 145 km) of 2493 km and a gravitational acceleration at the ocean center ≈ 1.25 m s^{-2}. A more exact result is given in equation (124) of *Beuthe* [2015b]. While the resonance occurs when $H_{\rm ocean} \sim H_{\rm res}$, an increase in the real part of h_2 can be seen even if the ocean thickness is several kilometers (Figure 3). Thus, a static formulation would give a sufficiently

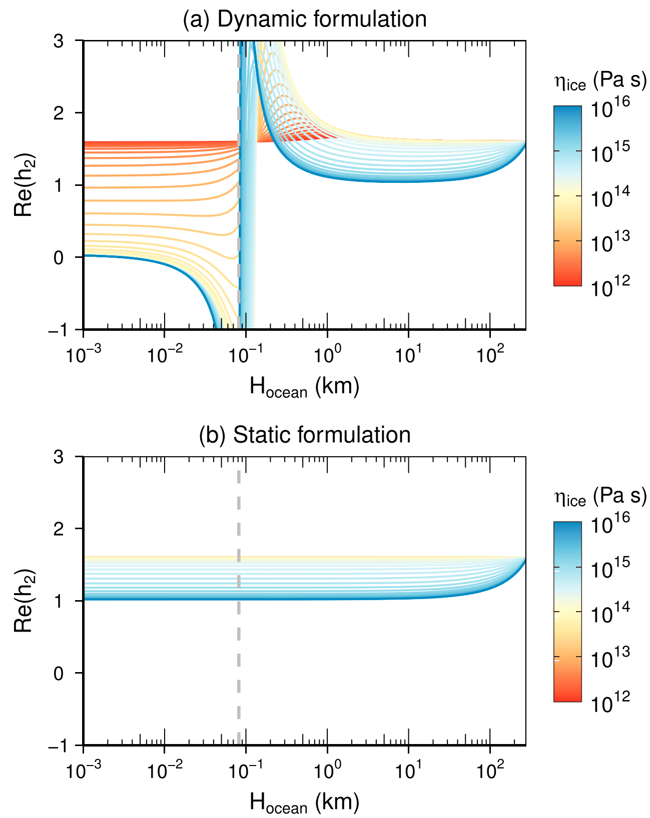

Figure 3. Real part of the degree 2 Love number h_2 as a function of ocean thickness for a Ganymede model. The vertical dashed lines indicate the resonant thickness $H_{res} \approx 81.8$ m estimated from equation (18). (a) A dynamic formulation results in a tidal resonance when $H_{ocean} \sim H_{res}$ while (b) a static formulation leads to no resonance. Under this model configuration, a static formulation leads to accurate results only when $H_{ocean} > 1$ km, much thicker than H_{res}.

accurate result only if $H_{ocean} \gg H_{res}$; a dynamical formulation should be used unless $H_{ocean} \gg H_{res}$. We note that calculations using a dynamical formulation are stable even if $H_{ocean} \gg H_{res}$, indicating that a wider range of parameters values can be adopted when the dynamic formulation is used.

The above result highlights the fact that a static formulation implicitly requires that the subsurface ocean is much thicker than the resonant thickness. This assumption, however, may not be satisfied for small icy satellites of giant planets. Figure 4 shows the resonant thickness H_{res} for major icy satellites, calculated from equation (18). Here we use the surface values of r and g, and the radius and mean density are taken from *Chen et al.* [2014]. The resonant thickness H_{res} for Mimas, Tethys, Miranda, and Enceladus is ~588, 457, 298, and 253 m, respectively. Although the minimum ocean thickness that gives sufficiently accurate results under a static formulation depends on properties of satellites (i.e., orbital period, gravity, and physical properties), the above results imply that such a critical thickness would be at least 10 km for these satellites. This result suggests that an application of a dynamic formulation may lead to a result different from previous studies using a static formulation for thin ocean models [e.g., *Roberts and Nimmo*, 2008; *Shoji et al.*, 2014], though a detailed comparison with such studies is beyond the scope of this study.

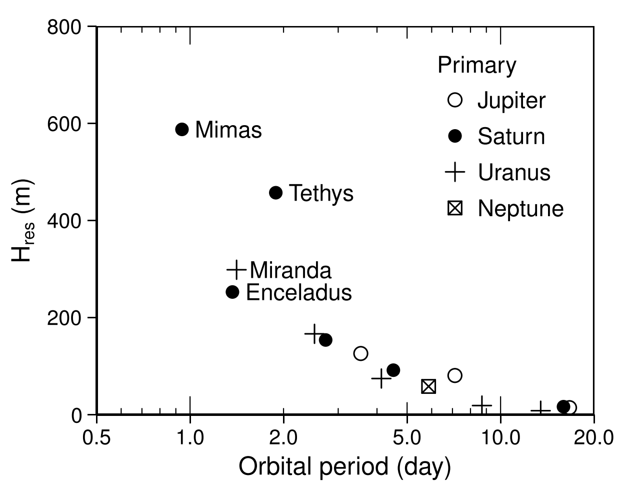

Figure 4. Resonant thickness H_{res} as a function of orbital period for major satellites of giant planets. Equation (18) is used. Values are taken from *Chen et al.* [2014].

We note that a resonant behavior caused by an internal liquid layer is similar to the free core nutation [e.g., *Van Hoolst et al.*, 2003], though the time evolution of rotational axis is not considered in this study. Further discussions will be given in section 5.

4. Effect of a Lid on Tidal Resonance

The results presented above suggest that the solid lid plays an important role in the tidal response of the ocean and the body as a whole. Below we investigate the effect of varying lid parameters on the resonant configuration. In order to emphasize the effect of the solid lid on resonance, we use a

Table 2. Model Parameters for Enceladus

Symbol	Quantity	Value	Unit
r_s	Radius of Enceladus	252.1	km
ρ_m	Mean density	1610	kg m^{-3}
ρ_{H_2O}	Density of the shell and ocean	1000	kg m^{-3}
μ_s	Rigidity of the shell	4.00	GPa
μ_m	Rigidity of the mantle	6.78	GPa
ω_{orb}	Orbital frequency	5.31×10^{-5}	rad s^{-1}

simple three-layer Enceladus model, consisting of a solid shell, a liquid ocean, and a solid mantle (Figure 1, right). For our nominal case, an incompressible limit (i.e., $\lambda \rightarrow \infty$) is assumed. The icy shell and mantle are assumed to be a Maxwell viscoelastic body and a Hookean elastic body, respectively. Free parameters are the viscosity η_{ice} of the top icy shell, the thickness D_{shell} of the top shell, and that H_{ocean} of the subsurface ocean. Table 2 summarizes parameter values, mainly adopted from *Matsuyama* [2014]. The density of the mantle is determined from the mean density (i.e., 1610 kg m^{-3}) and its radius, which is a function of D_{shell} and H_{ocean}. In what follows, we refer to situations in which the effect of the lid is ignored as a "surface ocean" case.

Figure 5 shows the absolute value of the gravitational Love number for degree 2, k_2, as a function of ocean thickness. Here k_2 is calculated from $k_2 = y_5(r_s)/\Phi_t - 1$. This figure demonstrates the effect of a lid overlying an ocean on the tidal resonance. First, no sharp increase in $|k_2|$ is found when η_{ice} is extremely low (i.e., 10^{11} Pa s) and D_{shell} is large. Under this condition, the icy shell behaves as a thick fluid layer. As a result, the "effective ocean thickness" of the satellite is given by $D_{shell} + H_{ocean}$, which is not small. Consequently, even if H_{ocean}

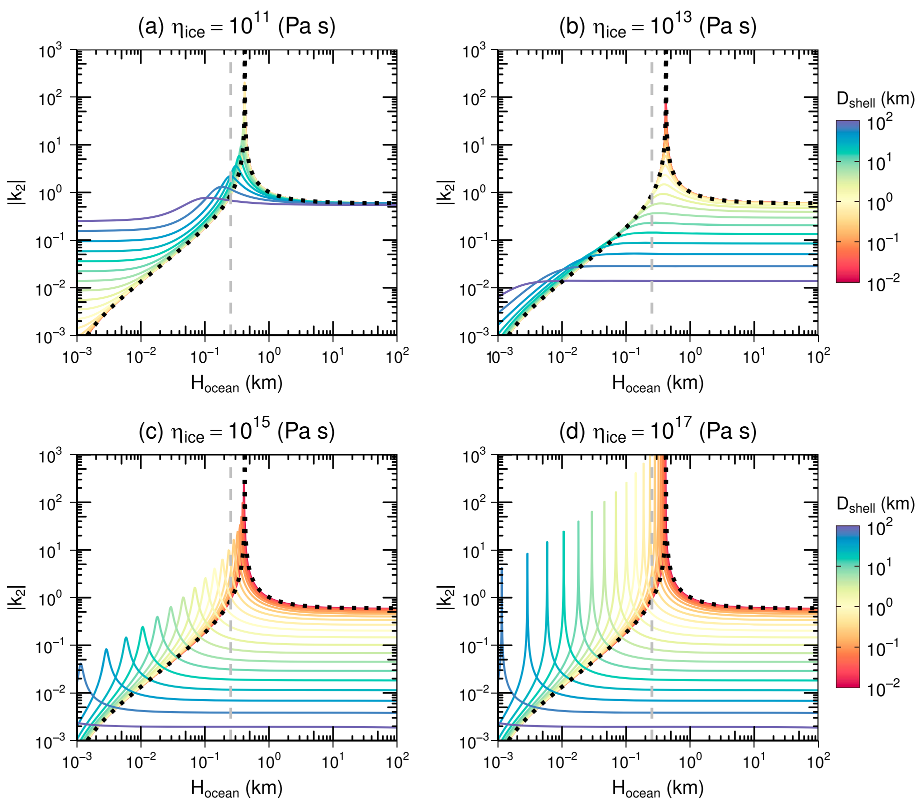

Figure 5. Absolute value of the degree 2 gravitational Love number k_2 as a function of ocean thickness for an incompressible Enceladus model. Results for a shell viscosity η_{ice} of (a) 10^{11} Pa s, (b) 10^{13} Pa s, (c) 10^{15} Pa s, and (d) 10^{17} Pa s are shown. The dotted curves are results for a surface ocean case ($D_{shell} = 0$ km). The vertical dashed lines indicate the resonant thickness $H_{res} \approx 253$ m estimated from equation (18). A resonance occurs if the shell thickness D_{shell} is small and/or the shell viscosity η_{ice} is high. Note that extremely high values of $|k_2|$ seen at resonant configurations are physically unlikely and violate the small-amplitude deformation assumption.

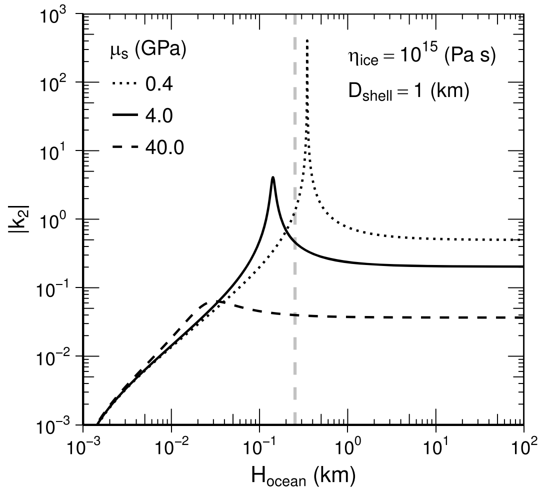

Figure 6. Absolute value of the degree 2 gravitational Love number k_2 as a function of ocean thickness for an incompressible Enceladus model. Results for a shell viscosity η_{ice} of 10^{15} Pa s and a shell thickness D_{shell} of 1 km are shown. The vertical dashed lines indicate the resonant thickness $H_{res} \approx 253$ m estimated from equation (18).

is small, a resonance does not occur (Figures 5a and 5b). For the case of $\eta_{ice} = 10^{13}$ Pa s with a large D_{shell}, no increase in $|k_2|$ is seen because of large dissipation in the shell.

In contrast, if D_{shell} is small (i.e., <1 km) or η_{ice} is moderate or high (i.e., $\geq 10^{15}$ Pa s), there is always one resonant configuration (Figures 5c and 5d). For a given D_{shell}, an increase in η_{ice} leads to a sharper resonant peak. This is because an increase in η_{ice} corresponds to an increase in the quality factor Q of the body. In addition, for a given η_{ice}, an increase in D_{shell} leads to a smaller resonant ocean thickness. Because of nonzero rigidity, an icy shell acts as a membrane resisting deformation. This is similar in principle to surface tension acting at a liquid surface. The phase velocity v_{grav} of gravity waves taking surface tension into account is given by

$$v_{grav} \approx \sqrt{gH_{ocean}\left(1 + \frac{T}{\rho g}k^2\right)}, \qquad (19)$$

where T is surface tension [e.g., *Lamb*, 1932]. Here we use a shallow water approximation: $\tanh(kH) \approx kH$ ($kH \ll 1$). This equation may be compared with equation (123) of *Beuthe* [2015b]. Equation (19) indicates that in order to produce the same v_{grav}, an increase in T requires a decrease in H_{ocean}. In a similar fashion, in our results the effect of this "membrane" increases with increasing D_{shell}; a thicker lid requires a thinner ocean thickness for a resonance to occur. Similarly, this membrane effect increases with increasing rigidity μ_s of a shell, leading to a thinner resonant ocean thickness as shown in Figure 6. The amount of this shift in the resonant thickness can be very large, even by a factor of >100.

We also investigated the effect of compressibility. Figure 7 shows results for different values of the first Lamé's parameter for the shell (λ_s) and illustrates that an increase in λ_s leads to a smaller resonant thickness and a smaller value of the Love number (k_2). This trend is similar to that seen in Figure 6 where we change rigidity (μ_s), supporting a surface tension interpretation for the effect of a lid on tidal resonance.

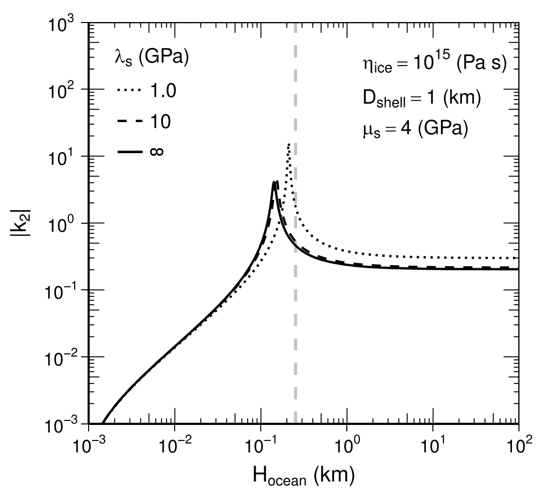

Figure 7. Absolute value of the degree 2 gravitational Love number k_2 as a function of ocean thickness for a compressible Enceladus model. Results for a shell viscosity η_{ice} of 10^{15} Pa s, a shell thickness D_{shell} of 1 km, and a shell rigidity μ_s of 4 GPa are shown. The vertical dashed lines indicate the resonant thickness $H_{res} \approx 253$ m estimated from equation (18).

5. Discussion

As discussed in section 4, as the role of the lid becomes more important, the resonant ocean thickness becomes smaller. This indicates that our estimate of the resonant thickness using equation (18)—which ignores lid effects—should be considered as the upper limit. We found only one resonant configuration (i.e., one ocean thickness) for a given set of shell properties. In contrast, previous studies with more complex ocean dynamics, but neglecting the role of the lid, found several resonant configurations [*Tyler*, 2011; *Matsuyama*, 2014]. The major difference between such studies and our surface ocean case is whether Coriolis forces are taken into account or not. In order to examine

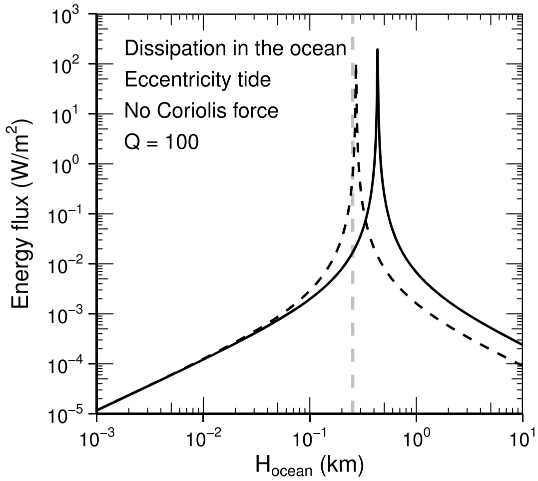

Figure 8. Energy flux due to tidal dissipation in the ocean as a function of ocean thickness for an incompressible Enceladus model. Results are obtained using a code developed by *Matsuyama* [2014], though Coriolis forces are removed. A quality factor Q for the ocean of 100 is adopted. The vertical dashed lines indicate the resonant thickness $H_{res} \approx 253$ m estimated from equation (18). The solid and dashed curves show results including and excluding the effects of ocean loading, self-attraction, and deformation of the solid regions, respectively. The resonant thickness for the former and the latter is ~430 m and ~270 m, respectively.

the effect of Coriolis forces, we calculate tidal dissipation in a surface ocean using the same code as *Matsuyama* [2014] but removing the effect of Coriolis forces. Results for an incompressible Enceladus model are shown in Figure 8. As expected, only one resonant configuration is found, for an ocean thickness ~430 m. This value is similar to the one found here for a surface ocean case, ~420 m (Figure 5). We note that this resonant thickness differs from the largest resonant thickness for the case with Coriolis forces taken into account, ~570 m [*Matsuyama*, 2014]. Consequently, Coriolis forces introduce several minor resonant configurations and shift the major resonant configuration. Figure 8 also shows the result of removing the effects of Coriolis forces, ocean loading, self-attraction, and deformation of the solid regions. In this case, the resonant ocean thickness is ~270 m, similar to the value estimated from equation (18), ≈253 m. This is consistent with the fact that this equation does not include such effects.

A recent study considers the tidal response on icy satellites with dynamical subsurface oceans [*Beuthe*, 2015b]. Assuming a rigid mantle and an incompressible subsurface ocean, nonnegligible inertial effects are found for Europa (unless a subsurface ocean is thicker than 20 km) but not for Titan. His model also found a resonance around $H_{ocean} \sim 0.1$ km, which is consistent with our results; again, equation (18) gives a good approximation for the resonant configuration as long as the effect of a solid lid is not extremely large.

It should be noted that the extremely large values of Love numbers near resonance are physically unlikely. As a subsurface ocean becomes thinner and approaches a resonant configuration, the amount of tidally produced heat would increase. Such an increase in the amount of heat would lead to a thickening of the ocean; it is therefore unlikely that the ocean thickness reaches the resonant thickness. On the other hand, large deformation of a shell overlying a thin ocean may result in the base of the shell locally coming into contact with the solid layer beneath. Equally, spatial variations in the equilibrium shell thickness owing to variations in tidal heating [e.g., *Nimmo et al.*, 2007] may cause local grounding of the shell. Neither situation is considered in this study since a global ocean is assumed. If the shell is in contact with the lower solid layer at some locations, the tidal response will likely be quite different [e.g., *Tobie et al.*, 2008; *Běhounková et al.*, 2012].

In addition, even if a subsurface ocean is global, lateral variations in physical properties in the shell may have an effect on tidal response; in such cases, components other than degree 2 would appear [e.g., *A et al.*, 2014]. To quantify the effect of such lateral variations, 3-D modeling is necessary. Furthermore, large-amplitude deformation of the kind which arises near resonance violates the assumption of small-amplitude deformation on which our analysis is based.

Nevertheless, these caveats do not imply that tidal resonance is not important. As noted above, a large increase in tidal heating rate is expected near the resonant configuration. Such a strongly varying tidal heating rate is more likely to give rise to periodic behavior than smoothly varying cases. For example, a case in which no heating at all occurs until the tidal stresses exceed a threshold produces strongly periodic behavior [*Stevenson*, 2008]. Thus, tidal resonance may not only quantitatively but also qualitatively affect the evolution of icy satellites possessing a subsurface ocean [*Tyler*, 2008; *Matsuyama*, 2014].

While Coriolis forces, ocean loading, self-attraction, and deformation of the solid regions do affect the major resonant configuration, the difference in terms of resonant ocean thickness are small (i.e., by a factor $< \sim 2$) [*Matsuyama*, 2014]. In contrast, as shown above, the effect of a lid can be much larger; the resonant thickness can differ by a factor of >100 if the lid is thick and stiff, demonstrating the importance of a lid on tidal resonance. Nevertheless, our model may overestimate the effect of a lid since we assume that the shell has a uniform viscosity structure for simplicity. The viscosity of an icy shell of actual satellites, however, would vary largely with depth [e.g., *Hussmann et al.*, 2007]; the viscosity of the near-surface layer would be very high while that of the base of the shell would be much lower. Consequently, the thickness of a stiff lid may be much thinner than that of the icy shell. In addition, we assume a zero viscosity ocean; tidal dissipation in the ocean is not modeled in this study. In an actual body with a subsurface ocean, however, tidal dissipation occurs in both the solid and liquid parts. Further studies considering a depth-dependent viscosity structure and combining tidal dissipation both in the solid and liquid would be important to better understand the role of tidal heating on planetary evolution.

6. Conclusion

In this study, we revisited the formulation for tidal deformation based on viscoelasto-gravitational theory and examined inertial effects. We found that a dynamic ocean formulation leads to a resonance while a static ocean formulation does not. This resonance would be important for a satellite with a thin (i.e., <1 km) subsurface ocean since it would lead to significantly enhanced tidal heating in the solid lid. The static ocean formulation, which has been used in previous tidal dissipation studies, would give an accurate Love number only if the ocean thickness is larger than the resonant thickness by a factor of several 10 (or >1 km). The resonant configuration strongly depends on properties of the shell; a higher shell viscosity leads to a sharper resonant configuration, and a thicker or more rigid shell leads to a thinner resonant ocean thickness. For tidal dissipation in the ocean, addition of the Coriolis force introduces additional minor resonant configurations and slightly shifts the major resonant configuration. This shift is much smaller than that caused by the presence of a thick or rigid shell. These results highlight the importance of the effects of a solid lid for tidal dissipation in icy satellites with subsurface oceans.

Appendix A: Governing Equation System Under the Incompressible Limit

The equation system for a solid layer is given by

$$\frac{\mathrm{d}y_1}{\mathrm{d}r} = -\frac{2}{r}y_1 + \frac{n(n+1)}{r}y_3, \tag{A1}$$

$$\frac{\mathrm{d}y_2}{\mathrm{d}r} = \left(-\omega^2\rho + \frac{12\tilde{\mu}}{r^2} - \frac{4\rho g}{r}\right)y_1 + \frac{n(n+1)}{r}\left(\rho g - \frac{6\tilde{\mu}}{r}\right)y_3 + \frac{n(n+1)}{r}y_4 + \frac{(n+1)\rho}{r}y_5 - \rho y_6, \text{ and} \tag{A2}$$

$$\frac{\mathrm{d}y_4}{\mathrm{d}r} = \left(\frac{\rho g}{r} - \frac{6\tilde{\mu}}{r^2}\right)y_1 - \frac{1}{r}y_2 + \left\{-\omega^2\rho + \frac{4n(n+1)\tilde{\mu}}{r^2} - \frac{2\tilde{\mu}}{r^2}\right\}y_3 - \frac{3}{r}y_4 - \frac{\rho}{r}y_5. \tag{A3}$$

The others remain the same (see equations (4)–(9)).

The equation system for a liquid layer is given by

$$\frac{\mathrm{d}y_1}{\mathrm{d}r} = \left\{-\frac{2}{r} + \frac{n\,(n+1)\,g}{\omega^2 r^2}\right\}y_1 - \frac{n\,(n+1)}{\omega^2\rho r^2}y_2 - \frac{n\,(n+1)}{\omega^2 r^2}y_5. \tag{A4}$$

The others remain the same (see equations (11)–(14)).

Appendix B: Initial Values

The differential equation systems are solved numerically assuming solutions of a homogeneous sphere for initial values y_i at a small value of r.

B1. Solid Core

The solution for spheroidal deformation of a compressible homogeneous solid sphere is given by a superposition of three solutions [e.g., *Love*, 1911; *Takeuchi and Saito*, 1972]. Because only the ratios between y_i are needed to be specified, we can use

$$y_1 = -\frac{f}{r} z_n(x), \tag{B1}$$

$$y_2 = -\rho f \alpha^2 k^2 + \frac{2\tilde{\mu}}{r^2} \left\{ 2f + n(n+1) \right\} z_n(x), \tag{B2}$$

$$y_3 = \frac{1}{r} z_n(x), \tag{B3}$$

$$y_4 = \mu k^2 - \frac{2\tilde{\mu}}{r^2}(f+1) z_n(x), \tag{B4}$$

$$y_5 = 3\gamma f - h\left(n\gamma - \omega^2\right), \tag{B5}$$

$$y_6 = \frac{2n+1}{r} y_5 \tag{B6}$$

for the first two sets of solutions and

$$y_1 = \frac{n}{r}, \tag{B7}$$

$$y_2 = \frac{2\tilde{\mu} n(n-1)}{r^2}, \tag{B8}$$

$$y_3 = \frac{1}{r}, \tag{B9}$$

$$y_4 = \frac{2\tilde{\mu}(n-1)}{r^2}, \tag{B10}$$

$$y_5 = n\gamma - \omega^2, \tag{B11}$$

$$y_6 = \frac{2n+1}{r} y_5 - \frac{3n\gamma}{r} \tag{B12}$$

for the third solution where

$$k_\pm^2 = \frac{1}{2}\left\{ \frac{\omega^2 + 4\gamma}{\alpha^2} + \frac{\omega^2}{\beta^2} \pm \sqrt{\left(\frac{\omega^2}{\beta^2} - \frac{\omega^2 + 4\gamma}{\alpha^2}\right)^2 + \frac{4n(n+1)\gamma^2}{\alpha^2 \beta^2}} \right\}, \tag{B13}$$

$$z_n(x) = \frac{x j_{n+1}(x)}{j_n(x)}, \quad x = kr, \quad f(k) = \frac{\beta^2 k^2 - \omega^2}{\gamma}, \quad h = f - (n+1), \tag{B14}$$

$$\alpha^2 = \frac{\tilde{\lambda} + 2\tilde{\mu}}{\rho}, \quad \beta^2 = \frac{\tilde{\mu}}{\rho}, \quad \gamma = \frac{4\pi}{3} G\rho, \tag{B15}$$

and j_n is the spherical Bessel function of degree n. Negative k^2 values are accepted [see *Love*, 1911, chapter VII]. The factor $z_n(x)$ is calculated from the recursion formula,

$$z_{n-1}(x) = \frac{x^2}{(2n+1) - z_n(x)}, \tag{B16}$$

and the calculation should be start from a sufficiently large n [*Takeuchi and Saito*, 1972]. The initial value of $z_n(x)$ for a large n is given by $z_n(x) = x^2/(2n+3)$.

When the medium is incompressible (i.e., $\lambda \to \infty; \alpha^2 \to \infty$), we find that $f(k_+) \to 0$ and $f(k_+)\alpha^2 k_+^2 = n(n+1)\gamma$. Consequently, the first set of initial values is given by

$$y_1 = 0, \tag{B17}$$

$$y_2 = n(n+1)\left\{-\rho\gamma + \frac{2\tilde{\mu}}{r^2} z_n(x)\right\}, \tag{B18}$$

$$y_3 = \frac{1}{r} z_n(x), \tag{B19}$$

$$y_4 = \tilde{\mu}\left\{\frac{\omega^2}{\beta^2} - \frac{2}{r^2} z_n(x)\right\}, \tag{B20}$$

$$y_5 = (n+1)\left(n\gamma - \omega^2\right), \text{ and} \tag{B21}$$

$$y_6 = \frac{2n+1}{r} y_5. \tag{B22}$$

Similarly, we find that $\alpha^2 k_-^2 \to \omega^2 + 4\gamma - n(n+1)\gamma^2/\omega^2$, $f(k_-) \to -\omega^2/\gamma$, $z(x) \to 0$. Consequently, the second set of initial values is given by

$$y_1 = 0, \tag{B23}$$

$$y_2 = \rho\left\{\frac{\omega^2}{\gamma}\left(\omega^2 + 4\gamma\right) - n(n+1)\gamma\right\}, \tag{B24}$$

$$y_3 = 0, \tag{B25}$$

$$y_4 = 0, \tag{B26}$$

$$y_5 = (h-3)\,\omega^2 - nh\gamma, \text{ and} \tag{B27}$$

$$y_6 = \frac{2n+1}{r} y_5. \tag{B28}$$

The third set of initial values remains the same.

B2. Liquid Core ($\mu \to 0$)

In this case, two sets of initial values for y_i ($i = 1, 2, 5, 6$) are required. We find that the form

$$y_1 = -\frac{f}{r} z_n(x), \tag{B29}$$

$$y_2 = -\rho\left\{f\left(\omega^2 + 4\gamma\right) + n(n+1)\gamma\right\}, \tag{B30}$$

$$y_5 = 3\gamma f - h\left(n\gamma - \omega^2\right), \text{ and} \tag{B31}$$

$$y_6 = \frac{2n+1}{r} y_5 \tag{B32}$$

for the first set of initial values and

$$y_1 = \frac{n}{r}, \tag{B33}$$

$$y_2 = 0, \tag{B34}$$

$$y_5 = n\gamma - \omega^2, \text{ and} \tag{B35}$$

$$y_6 = \frac{2n+1}{r} y_5 - \frac{3n\gamma}{r} \tag{B36}$$

for the second set of initial values, respectively. Here

$$k^2 = \frac{1}{\alpha^2}\left\{\omega^2 + 4\gamma - \frac{n(n+1)\gamma^2}{\omega^2}\right\}, \quad f = -\frac{\omega^2}{\gamma}, h = f - (n+1), \quad \alpha^2 = \lambda/\rho. \tag{B37}$$

When $\alpha^2 \to \infty$, we find $k^2 \to 0$. Thus, for the first set of initial values, $y_1 = 0$, and the others remain the same. The second set of initial values also remains the same.

Appendix C: Profiles of *y* Functions

Here we provide an example of profiles of *y* functions. Results for the top 2 km of an incompressible Enceladus model are shown in Figures C1 (real part) and C2 (imaginary part). Calculation conditions are $\eta_{\rm ice} = 10^{15}$ Pa s, μ_s = 4 GPa, $D_{\rm shell}$ = 1 km, and $10^{-2} \le H_{\rm ocean} \le 1$ km. Absolute values of *y* increase as the ocean thickness

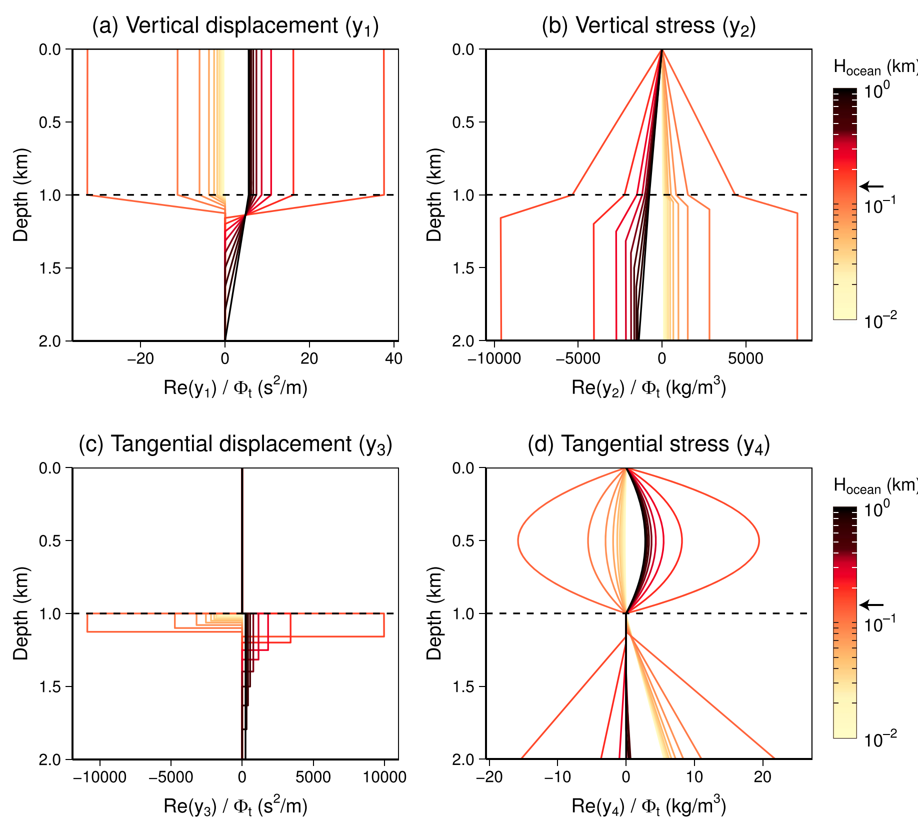

Figure C1. Profiles of the real part of *y* functions for an incompressible Enceladus model. Results for the top 2 km, $\eta_{\rm ice} = 10^{15}$ Pa s, $\mu_s = 4$ GPa, $D_{\rm shell} = 1$ km, and $10^{-2} \le H_{\rm ocean} \le 1$ km are shown. *y* functions are normalized by tidal potential Φ_t. The horizontal dashed lines indicate the boundary between the top ice shell and a subsurface ocean. The left arrows in legends indicate the resonant ocean thickness (≈140 m). Large absolute values particularly for y_3 in the ocean can be seen when $H_{\rm ocean}$ is close to the resonant ocean thickness.

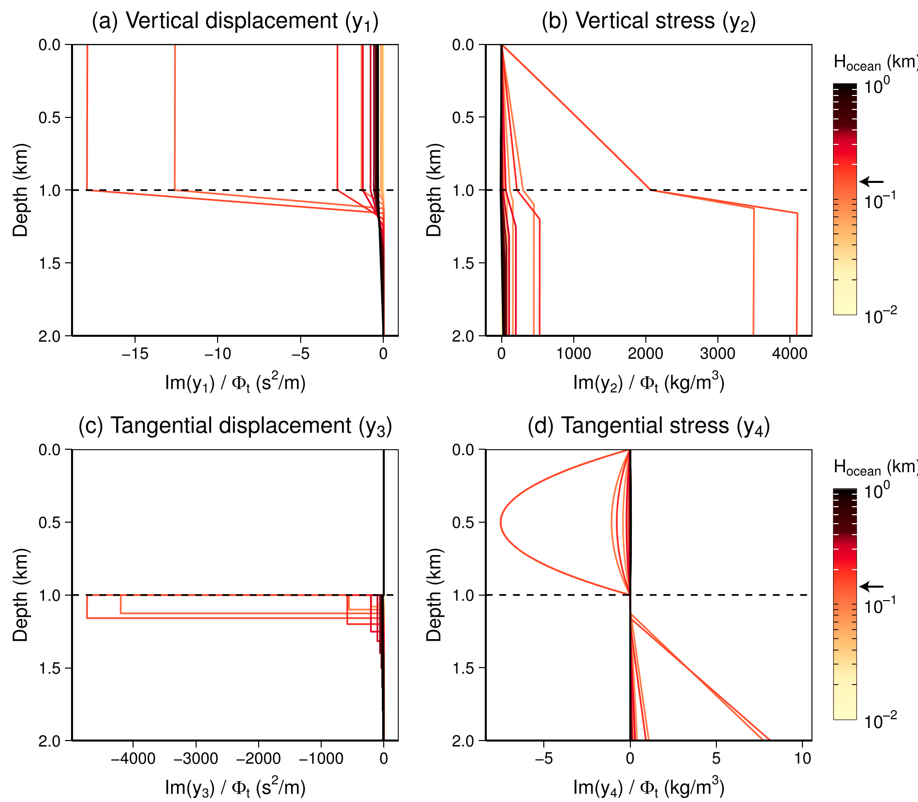

Figure C2. Profiles of the imaginary part of y functions for an incompressible Enceladus model. Calculation conditions are the same as adopted in Figure C1.

H_{ocean} approaches the resonant ocean thickness (≈140 m). In particular, y_3 in the ocean becomes very large at the resonant configuration. This result suggests that tidal dissipation in the ocean as well as friction at the solid-liquid boundary would lead to a large heat production when the ocean thickness is close to the resonant configuration.

Acknowledgments
We thank two anonymous reviewers for their careful reviews and constructive comments for improving this manuscript and J. Kimura and K. Matsumoto for fruitful discussions. Numerical data to produce figures in this paper are provided as supporting information. No actual field data are used. This study was partially supported by a MEXT grant for the tenure-tracking system.

References

A, G., J. Wahr, and S. Zhong (2013), Computations of the viscoelastic response of a 3-D compressible Earth to surface loading: An application to Glacial Isostatic Adjustment in Antarctica and Canada, *Geophys. J. Int.*, *192*, 557–572, doi:10.1093/gji/ggs030.

A, G., J. Wahr, and S. Zhong (2014), The effects of laterally varying icy shell structure on the tidal response of Ganymede and Europa, *J. Geophys. Res. Planets*, *119*, 659–678, doi:10.1002/2013JE004570.

Alterman, Z., H. Jarosch, and C. L. Pekeris (1959), Oscillations of the Earth, *Proc. R. Soc. A*, *252*, 80–95, doi:10.1098/rspa.1959.0138.

Anderson, J. D., E. L. Lau, W. L. Sjogren, G. Schubert, and W. B. Moore (1996), Gravitational constraints on the internal structure of Ganymede, *Nature*, *384*, 541–543, doi:10.1038/384541a0.

Barr, A. C., and G. C. Collins (2015), Tectonic activity on Pluto after the Charon-forming impact, *Icarus*, *246*, 146–155, doi:10.1016/j.icarus.2014.03.042.

Běhounková, M., G. Tobie, G. Choblet, and O. Čadek (2012), Tidally-induced melting events as the origin of south-pole activity on Enceladus, *Icarus*, *219*, 655–664, doi:10.1016/j.icarus.2012.03.024.

Beuthe, M. (2015a), Tides on Europa: The membrane paradigm, *Icarus*, *248*, 109–134, doi:10.1016/j.icarus.2014.10.027.

Beuthe, M. (2015b), Tidal Love numbers of membrane worlds: Europa, Titan, and Co., *Icarus*, *258*, 239–266, doi:10.1016/j.icarus.2015.06.008.

Chen, E., F. Nimmo, and G. Glatzmaier (2014), Tidal heating in icy satellite oceans, *Icarus*, *229*, 11–30, doi:10.1016/j.icarus.2013.10.024.

Dahlen, F. A., and J. Tromp (1998), *Theoretical Global Seismology*, Princeton Univ. Press, Princeton.

Harada, Y., S. Goossens, K. Matsumoto, J. Yan, J. Ping, H. Noda, and J. Haruyama (2014), Strong tidal heating in an ultralow-viscosity zone at the core-mantle boundary of the Moon, *Nat. Geosci.*, *7*, 569–572, doi:10.1038/ngeo2211.

Hemingway, D., F. Nimmo, H. Zebker, and L. Iess (2013), A rigid and weathered ice shell on Titan, *Nature*, *500*, 550–552, doi:10.1038/nature12400.

Hussmann, H., C. Sotin, and J. Lunine (2007), Interiors and evolution of icy satellites, in *Treatise on Geophysics*, edited by G. Schubert, pp. 509–539, Elsevier, Amsterdam, Netherlands., doi:10.1016/B978-044452748-6.00168-1

Iess, L., R. A. Jacobson, M. Ducci, D. J. Stevenson, J. I. Lunine, J. W. Armstrong, S. W. Asmar, P. Racioppa, N. J. Rappaport, and P. Tortora (2012), The tides of Titan, *Science*, *337*, 457–459, doi:10.1126/science.1219631.

Iess, L., D. J. Stevenson, M. Parisi, D. Hemingway, R. A. Jacobson, J. I. Lunine, F. Nimmo, J. W. Armstrong, S. W. Asmar, M. Ducci, and P. Tortora (2014), The gravity field and interior structure of Enceladus, *Science*, *344*, 78–80, doi:10.1126/science.1250551.

Jara-Orué, H. M., and B. L. A. Vermeersen (2011), Effects of low-viscous layers and a non-zero obliquity on surface stresses induced by diurnal tides and non-synchronous rotation: The case of Europa, *Icarus*, *215*, 417–438, doi:10.1016/j.icarus.2011.05.034.

Kivelson, M., K. Khurana, and M. Volwerk (2002), The permanent and inductive magnetic moments of Ganymede, *Icarus*, *157*, 507–522, doi:10.1006/icar.2002.6834.

Kivelson, M. G., K. K. Khurana, C. T. Russell, M. Volwerk, R. J. Walker, and C. Zimmer (2000), Galileo magnetometer measurements: A stronger case for a subsurface ocean at Europa, *Science*, *289*, 1340–1343, doi:10.1126/science.289.5483.1340.

Lamb, H. (1932), *Hydrodynamics*, 6th ed., Cambridge Univ. Press, Cambridge, U. K.

Love, A. E. H. (1911), *Some Problems of Geodynamics*, Cambridge Univ. Press, Cambridge, U. K.

Matsuyama, I. (2014), Tidal dissipation in the oceans of icy satellites, *Icarus*, *242*, 11–18, doi:10.1016/j.icarus.2014.07.005.

Moore, W. B., and G. Schubert (2000), The tidal response of Europa, *Icarus*, *147*, 317–319, doi:10.1006/icar.2000.6460.

Moore, W. B., and G. Schubert (2003), The tidal response of Ganymede and Callisto with and without liquid water oceans, *Icarus*, *166*, 223–226, doi:10.1016/j.icarus.2003.07.001.

Nimmo, F., P. Thomas, R. Pappalardo, and W. Moore (2007), The global shape of Europa: Constraints on lateral shell thickness variations, *Icarus*, *191*, 183–192, doi:10.1016/j.icarus.2007.04.021.

Roberts, J. H., and F. Nimmo (2008), Tidal heating and the long-term stability of a subsurface ocean on Enceladus, *Icarus*, *194*, 675–689, doi:10.1016/j.icarus.2007.11.010.

Robuchon, G., and F. Nimmo (2011), Thermal evolution of Pluto and implications for surface tectonics and a subsurface ocean, *Icarus*, *216*, 426–439, doi:10.1016/j.icarus.2011.08.015.

Sabadini, R., and B. Vermeersen (2004), *Global Dynamics of the Earth: Applications of Normal Mode Relaxation Theory to Solid-Earth Geophysics*, Springer, Dordrecht, Netherlands,

Saito, M. (1974), Some problems of static deformation of the Earth, *J. Phys. Earth*, *22*, 123–140.

Saur, J., et al. (2015), The search for a subsurface ocean in Ganymede with Hubble Space Telescope observations of its auroral ovals, *J. Geophys. Res. Space Physics*, *120*, 1715–1737, doi:10.1002/2014JA020778.

Schubert, G., T. Spohn, and R. T. Reynolds (1986), Thermal histories, compositions and internal structures of the moons of the solar system, in *Satellites*, edited by J. A. Burns and M. S. Matthews, pp. 224–292, Univ. Ariz. Press, Tucson.

Schubert, G., J. D. Anderson, T. Spohn, and W. B. McKinnon (2004), Interior composition, structure and dynamics of the Galilean satellites, in *Jupiter: The Planet, Satellites and Magnetosphere*, edited by F. Bagenal, T. E. Dowling, and W. B. McKinnon, pp. 281–306, Cambridge Univ. Press, Cambridge, U. K.

Schubert, G., H. Hussman, V. Lainey, D. L. Matson, W. B. McKinnon, C. Sotin, G. Tobie, D. Turrini, and T. Van Hoolst (2010), Evolution of icy satellites, *Space Sci. Rev.*, *153*, 447–484, doi:10.1007/s11214-010-9635-1.

Schulson, E. M., and P. Duval (2009), *Creep and Fracture of Ice*, Cambridge Univ. Press, Cambridge, U. K.

Shoji, D., H. Hussmann, F. Sohl, and K. Kurita (2014), Non-steady state tidal heating of Enceladus, *Icarus*, *235*, 75–85, doi:10.1016/j.icarus.2014.03.006.

Stevenson, D. J. (2008), Constraints on tidal heating in Enceladus, *Eos Trans. AGU*, *89*(53), Fall Meet. Suppl., Abstract P13D–04.

Tajeddine, R., N. Rambaux, V. Lainey, S. Charnoz, A. Richard, A. Rivoldini, and B. Noyelles (2014), Constraints on Mimas' interior from Cassini ISS libration measurements, *Science*, *346*, 322–324, doi:10.1126/science.1255299.

Takeuchi, H., and M. Saito (1972), Seismic surface waves, *Methods Comput. Phys.*, *11*, 217–295.

Tobie, G., A. Mocquet, and C. Sotin (2005), Tidal dissipation within large icy satellites: Applications to Europa and Titan, *Icarus*, *177*, 534–549, doi:10.1016/j.icarus.2005.04.006.

Tobie, G., O. Čadek, and C. Sotin (2008), Solid tidal friction above a liquid water reservoir as the origin of the south pole hotspot on Enceladus, *Icarus*, *196*, 642–652, doi:10.1016/j.icarus.2008.03.008.

Tyler, R. (2008), Strong ocean tidal flow and heating on moons of the outer planets, *Nature*, *456*, 770–772, doi:10.1038/nature07571.

Tyler, R. (2011), Tidal dynamical considerations constrain the state of an ocean on Enceladus, *Icarus*, *211*, 770–779, doi:10.1016/j.icarus.2010.10.007.

Van Hoolst, T., V. Dehant, F. Roosbeek, and P. Lognonné (2003), Tidally induced surface displacements, external potential variations, and gravity variations on Mars, *Icarus*, *161*(2), 281–296, doi:10.1016/S0019-1035(02)00045-3.

Zschau, J. (1978), Tidal friction in the solid Earth: Loading tides versus body tides, in *Tidal Friction and the Earth's Rotation*, edited by P. Brosche and J. Suendermann, pp. 62–94, Springer, New York.